Nano Express

Graphene modulated $LiMn_{1.5}Ni_{0.4}Cr_{0.1}O_4$ spinel cathode for lithium ion battery

To cite this article before publication: Rajesh K Katiyar *et al* 2020 *Nano Ex.* in press https://doi.org/10.1088/2632-959X/abadda

Graphene modulated $LiMn_{1.5}Ni_{0.4}Cr_{0.1}O_4$ spinel cathode for Lithium ion Battery

Rajesh K. Katiyar,[1] Balram Tripathi[1] , Javier Palomino,[1] Atul Tiwari[3] , Shiva Adireddy [4], Ambesh Dixit[5], Brad R. Weiner[2], Gerardo Morell[1] and Ram S. Katiyar[1]

[1] Institute of Functional Nanomaterials, Department of Physics, University of Puerto Rico, San Juan, PR 00931, USA

[2] Institute of Functional Nanomaterials, Department of Chemistry, University of Puerto Rico, San Juan, PR 00936, USA

[3] Strategic Research & Developments Pantheon Chemicals Inc. 225 W Deer Valley Road #4, Phoenix, 85027, AZ, USA

[4]Department of Physics and Engineering Physics, Tulane University, New Orleans- LA 70118, USA

[5]Department of Physics, Indian Institute of Technology, Jodhpur-342011, India

Abstract

We report the development of a rechargeable lithium ion battery with homogeneous mixing of 10 % of graphene oxide in active $LiMn_{1.5}Ni_{0.4}Cr_{0.1}O_4$ cathode material for enhanced electrochemical performance. The redox behavior of the cell, which is normally too slow for practical applications, is accelerated with highly conductive graphene. Intimate mixing of the two materials is achieved by a slurry maker using an organic solution for a cathode paste. The fabricated electrode is repeatedly charged/discharge at C/10 and C/2 rates without any significant degradation in the electrochemical capacity. The gravimetric energy density of the composite cathode material exceeds that of the $LiMn_{1.5}Ni_{0.4}Cr_{0.1}O_4$ oxide electrode in lithium-ion batteries, and the addition of graphene in active material is likely to prove advantageous in applications where weight, rather than volume, is a critical factor.

Keywords: Graphene, $LiMn_{1.5}Ni_{0.4}Cr_{0.1}O_4$ spinel, High energy, Rechargeable battery

*Corresponding Author Email: rkatiyar@hotmail.com

1. Introduction:

The development of low cost rechargeable lithium ions batteries is of considerable technological importance because of their relatively high energy densities. The rechargeable lithium ion batteries exhibit high theoretical energy storage capability with relatively lower weight and higher mechanical strength. Further, lithium-ion batteries (LIBs) with high energy density, design flexibility, and low weight are useful for energy storage, which have been widely used in various applications such as portable mobile electronic devices, hybrid electric vehicles, and military applications.[1-6]. Among LiMn2O4 spinel group materials, $LiMn_{1.5}Ni_{0.4}Cr_{0.1}O_4$ cathode materials has attracted attention as an efficient cathode material because of its high operating voltage, high specific capacity, and structural stability[7-9]. However, the poor electronic conductivity of $LiMn_{1.5}Ni_{0.4}Cr_{0.1}O_4$ cathode ends up with relatively lower electrochemical performance, thus restricting its practical applications. The conventional reaction synthesis method is not suitable for preparing low conductivity cathode materials in large scales for any practical applications.[10-11] Multilayer graphene powder may be a very good alternative additive to the active cathode material to realize the enhanced electronic conductivity through percolating network and also provide the structural stability simultaneously for high energy density and capacity of oxide materials [12-14].

There are some studies on highly conductive nano-structured carbon particles inserted in the active host materials, showing improved electronic conductivity and thereby enhance the discharge capacity as well as cycle stability at high current densities[15-16]. In order to achieve excellent structural stability with large surface-to-volume ratio and high electronic conductivity, highly conductive graphene electrode is added for the development of more efficient LIB [17-20] Also graphene leads to larger reversible capacity due to efficient Li intercalation between adjacent layers [21]. Graphene is the ideal material for blocking release of oxygen into the electrolyte. Graphene can effectively improve electron and ion transportation of the electrode materials, so the addition of graphene can greatly enhance lithium ion battery's properties and provide better chemical stability, higher electrical conductivity and higher capacity. It is impermeable to oxygen, electrically conductive, flexible, and is strong enough to withstand conditions within the battery. It is only a few nanometers thick so there would be no extra mass added to the battery. Our research shows that its use in the cathode can reliably reduce the release of oxygen and could be one way that the risk for fire in these batteries[22-26]. Improved surface conductivity, capacity, rate

capability, and cyclic stability of graphene-containing electrode materials are also confirmed for composite materials [27-29]. In the present work, we study the effect of adding graphene into $LiMn_{1.5}Ni_{0.4}Cr_{0.1}O_4$ cathode material to understand its impact on the electrochemical performance and charge/discharge cyclability.

2. Experiment Procedures:

The highly oriented pyrolytic graphite powder from (Alfa aesar) was added to a desired quantity of concentrated H_2SO_4 at room temperature and the mixture was continuously stirred for one hour. The container was transferred into an ice bath to lower the reaction temperature. This process was followed by the addition of potassium permanganate (KMnO4) slowly and the solution is allowed to mix thoroughly for few hours. A large quantity of distilled water was then added to the solution followed by the slow addition of hydrogen peroxide until the gas evolution has stopped. Further, excess water was added and the solution was filtered several times to get graphene oxide. A film of graphene oxide powder was deposited on the filter paper after filtration, which was isolated after drying properly. It was then placed on a manual motorized stage for laser heating using a 532 nm line of a diode laser (incident power was ~500 mW). This process resulted in reduced graphene oxide. It was further confirmed with Raman scattering, where noticed increase in the intensity of D peak as compared to that of G peak substantiated the successful reduction of graphene oxide. The $LiMn_{1.5}Ni_{0.4}Cr_{0.1}O_4$ cathode material was synthesized by a sol-gel method which is reported elsewhere[30]. The graphene and pure phase cathode powder were mixed in 10:90 weight ratio to get a graphene modulated $LiMn_{1.5}Ni_{0.4}Cr_{0.1}O_4$ active cathode materials. The phase purity and the crystallinity of the $LiMn_{1.5}Ni_{0.4}Cr_{0.1}O_4$ cathode material were investigated using a Siemens D5000 X-ray powder diffractometer [CuKα radiation, 1.5405 Å]. X-ray photoelectron spectroscopy (XPS) measurements of $LiMn_{1.5}Ni_{0.4}Cr_{0.1}O_4$ cathodes were performed before and after charge–discharge cycle, using PHI ESCA system (Physical Electronics) using Al Kα radiation. Curve fitting of the slow-scanned XPS spectra was carried out using a non-linear least-squares fitting program with a Gaussian–Lorentz sum function. The cathode slurry was prepared by mixing of graphene modulated $LiMn_{1.5}Ni_{0.4}Cr_{0.1}O_4$ active cathode material with polyvinylidene fluoride (weight ratio 95:5) in N-methyl pyrolidone (NMP). The resulting paste was casted uniformly onto aluminum foil followed by drying at about 60-70 oC in vacuum furnace overnight. The coin cells were fabricated in an argon atmosphere, inside a Glove Box (MBraun Inc., USA), using $LiMn_{1.5}Ni_{0.4}Cr_{0.1}O_4$

electrode as cathode, Li foil as anode, and 1 M lithium hexafluoride (LiPF6), dissolved in ethyl carbonate (EC) and dimethyl carbonate (DMC) [1:2, v/v ratio] as electrolyte. The electrochemical behavior of the cells was studied at room temperature by cyclic voltammetry and charge–discharge characteristics, using solartron battery tester, Model 1470E. The impedance measurements of the cells were carried out using Gamry Instruments potentiostat and EIS 300 electrochemical software.

3. Results and Discussion:

The XRD pattern of graphene modulated $LiMn_{1.5}Ni_{0.4}Cr_{0.1}O_4$ is shown in Figure 1. All diffraction peaks are indexed to cubic crystal structure with Fd3m space group and thus confirming the spinel structure. The sharpness of peaks is suggesting that the prepared material is well-crystallized [31]. Additionally, a carbon peak is also observed in XRD pattern of graphene modulated $LiMn_{1.5}Ni_{0.4}Cr_{0.1}O_4$ composite, substantiating the presence of graphene in cathode matrix [32-34]. However the superstructure peaks which are characteristics of Ni and Mn ordering cannot be resolved from the XRD patterns of the spinels because of their low intensities [35]. Therefore, further structural investigation by Raman is required to confirm the P4332 symmetry of the synthesized spinel. The recorded Raman spectra as shown in Figure (2a &2b) represents spectrum of $LiMn_{1.5}Ni_{0.4}Cr_{0.1}O_4$ and graphene modulated $LiMn_{1.5}Ni_{0.4}Cr_{0.1}O_4$ respectively. The Raman modes at 492 and 640 cm-1are assigned to Eg and A1g active Raman-modes for the transition metal oxygen arrangements in the spinel structure of lithium metal oxide with Fd3m symmetry [36-37]. The characteristic of cubic spinel Raman active modes at 600 cm-1 indicates that the material is a single phase spinel structure [38]. The characteristics spinel Raman modes are observed in range of 200-2500 cm-1 as shown in figure 2b for both pristine $LiMn_{1.5}Ni_{0.4}Cr_{0.1}O_4$ and graphene modulated $LiMn_{1.5}Ni_{0.4}Cr_{0.1}O_4$ samples. We clearly observed carbon Raman bands in graphene modulated $LiMn_{1.5}Ni_{0.4}Cr_{0.1}O_4$ sample, which is absent for pristine $LiMn_{1.5}Ni_{0.4}Cr_{0.1}O_4$ sample. The carbon bands of the graphene are de-convoluted further and shown in Figure 2(c). The peaks observed at 1361 and 1584 cm-1 correspond to D and G bands of graphene layer, respectively. The impurity peak i.e. D band arises due to the disorder induced sp2-bonded carbon, whereas G band arises from in-plane vibration of sp2 bonded carbon atoms in graphene [39]. The Raman spectrum of $LiMn_{1.5}Ni_{0.4}Cr_{0.1}O_4$ showing the strong band around 638 cm-1 is assigned to the symmetric Mn-O stretching mode of MnO6 octahedral (A1g) while the band at 498 cm-1 associated with the Ni2+-O stretching mode in the structure [40].

The surface morphology of the prepared $LiMn_{1.5}Ni_{0.4}Cr_{0.1}O_4$ was confirmed by FE-SEM as shown in Figure 3(a,b,c,d) at different magnifications. The pristine sample showed larger particles with sizes around 500–1000 nm, which are relatively larger than graphene modulated $LiMn_{1.5}Ni_{0.4}Cr_{0.1}O_4$ sample where particle size is limited to 200-300 nm in size. This suggests that inclusion of graphene reduces agglomeration of the $LiMn_{1.5}Ni_{0.4}Cr_{0.1}O_4$ system . The agglomerated polyhedral-shaped particles with sizes of 300-480 nm are observed in low- and high-magnification FE-SEM images of graphene modulated $LiMn_{1.5}Ni_{0.4}Cr_{0.1}O_4$ sample (Figure 3b-d). The low-magnification FE-SEM image of the cathode powder shows the polyhedral-shaped particles wrapped between the graphene sheets shown in Figure (3b).

A cyclic voltammetry (CV) is one of the most prominent techniques in order to study the redox behavior of electrochemical materials. The CV characteristics in the voltage range 3.0-4.9 V at a scanning rate of 0.01mV/s for graphene modulated $LiMn_{1.5}Ni_{0.4}Cr_{0.1}O_4$ cathode are shown in Figure 4. The voltammograms showed well-defined redox peaks along with an anodic peak centered at 3.7 V. This peak explains the oxidation of Mn3+/Mn4+ and another peaks correspond to nickel and chromium with respective 2+ and 3+ oxidation states indicating their perfect stoichiometry. These peaks are known to be electrochemically active and undergo redox transitions after few charge discharge cycles [30-31] . An indication of anodic peaks at 4.65 V in the first charge-discharge cycle corresponds to the oxidation of Ni2+ to Ni4+ via Ni3+[10-11] is probably due to redox couples of Ni2+/Ni3+ and Ni3+/Ni4+ and or Li vacancy ordering[41]. A continuous cycling at C/10 showed the disappearance of intense anodic peak at 4.65 V and appearance of distinguishable redox peaks in between 3.0–4.9 V in both charging as well as discharging cycles. The redox peaks were observed when the cells are charged at C/10, indicating the activation of graphene in the composite system. The smaller current density will increase the respective activation of graphene element in active cathode materials and thus, it will exhibits high capacity.

Further, the study of chemical state of graphene modulated $LiMn_{1.5}Ni_{0.4}Cr_{0.1}O_4$ were investigated by XPS. The collected elemental XPS binding energy curves for each element (Li1s, Mn3d, Mn3s, C1s, Cr2p, Mn2p, O1s, Ni2p) are shown in Fig. 5(a-g) for as prepared i.e. before and after charging as well. These data are calibrated with respect to C1s (284.6 eV) carbon elemental peak, as shown in figure 5(c). In addition to the C1s peak at 284.6 eV, another peak at around 288.75 eV [42] is observed, which has relatively lower intensity in pristine sample and became very intense in case

after electrochemical cycling. This is associated with the bonding of graphitic carbon to the oxygen atoms of cathode material. The de-intercalation of Li during charging is observed in Li1s region (Fig.5a), suggesting the presence of Li and the peak around 54.5 eV attributed to Li 1s [38] in transition metal oxide, consistent with our findings. The lithium 1s peak becomes more clear in after electrochemical cycle XPS spectra Fig. 5(a). The binding energy of We also noticed characteristic Mn3d ~ 48 eV, and Mn 3s between 85-90 eV XPS peaks Fig.5(b). The O1s spectra are shown in Fig.5(d) and two peaks ~ 531 eV and 528 eV are observed, which correspond to spinel O and interface or/and defect O. These are dominating features in the spectra before charging than after charging. These peaks are also present with reduced intensity in the XPS spectrum after electrochemical cycling XPS spectra, however a new peak has evolved at 535.5 eV. This high binding energy peak may correspond to the residual oxygen containing functional groups (such as -OH and -COOH) bonded with C atoms in graphene [43]. The Cr XPS spectrum is shown in Figure 5(e), showing the signature of Cr3+ peak, whereas no significant Cr6+ peak is observed (Fig.5e). The intensity of Cr2P peak is also very poor and is because of the very small atomic fraction of Cr in $LiMn_{1.5}Ni_{0.4}Cr_{0.1}O_4$ cathode material and relatively similar results are observed for after cycle XPS spectrum. Further, Mn2p XPS spectra is shown in Figure 5(f), showing dominant Mn4+ XPS peak with respect to Mn3+ in before charging case. The Mn3+ intense peak is observed after cycling and Mn4+ is relatively not seen (fig. 5f). A weak Ni2p (fig. 5g) XPS peaks were observed in both the samples with Ni 2p3/2 located at 853.3 eV and 2p1/2 at 871.7 eV with an energy splitting (Δ) = 18.4 eV, and results are consistent with the nickel positions in oxide materials. Interestingly, we noticed that XPS binding energy peaks for most of the elements are shifted to higher binding energy values after charging. The multiplet splitting observed in these elements is the consequence of the interaction between the spins of unpaired electrons in the valence levels i.e. in 3d-transition metals such as Cr and Mn, giving rise to the complex peak structure [33].

The electrochemical performance of graphene modulated $LiMn_{1.5}Ni_{0.4}Cr_{0.1}O_4$ composite electrode was evaluated at different discharge rate in 3.0 and 4.9 V. The electrochemical performance of the composite electrode without graphene has been tested and published by Katiyar et.al. [29]. The galvanostatic charge/discharge profiles at C/10 and C/2 current rates are shown in Figures 6, and 7, respectively. As shown in figure initially the voltage increases monotonically until 3.73 V and reaches in a plateau region between 3.73 and 4.56 V. We observed low capacity in the initial few cycles for graphene modulated $LiMn_{1.5}Ni_{0.4}Cr_{0.1}O_4$ whereas almost negligible irreversible loss is

noticed after a few cycles. The maximum discharge capacities observed was ~154 mAh/g at C/10 current rate at 3.73 V. The above characteristic revealed an enhancement of electrochemical performance in the active cathode material by the addition of graphene [13-22]. Similar discharge capacities observed in the >50 cycles indicate reversible nature with well ionic pathways de-intercalation of lithium ions in the cathode materials. Although there is a decrease in the discharge capacity of the samples upon increasing current rates, the $LiMn_{1.5}Ni_{0.4}Cr_{0.1}O_4$ electrode clearly shows low discharge capacity but enhanced stability >50 cycles. The extended cyclic stability measurements of the $LiMn_{1.5}Ni_{0.4}Cr_{0.1}O_4$ combined with the graphene electrodes conducted at different current rates are shown in Figure 7. Initially, low discharge capacity increased with increasing cycles due to more stable electronics and ionic path by graphene into structure and reached values very close to the theoretical capacity of 148 mAh/g. The cell showed improved discharge capacity at C/10 current rates after 50 charge cycles, while a negligible capacity fading was observed for $LiMn_{1.5}Ni_{0.4}Cr_{0.1}O_4$ combined with graphene at C/2 current rates that was ascribed to polarization effects. The $LiMn_{1.5}Ni_{0.4}Cr_{0.1}O_4$ combined with graphene at C/10 is retained >98% due to the more stable structure obtained by the addition of graphene. The high capacity of the cathode is due to increase in the electronic conductivity, which reduces the cell polarization and prevents the evolution of oxygen from the cathodes.

Electrochemical Impedance Spectroscopy (EIS) is a non-destructive technique and widely used to understand the electrode and electrolyte interfaces. To understand and the beneficial effect of graphene on the electrochemical performance of $LiMn_{1.5}Ni_{0.4}Cr_{0.1}O_4$ cathode, alternating-current (AC) impedance measurements are carried out after five charge discharge cycles at C/10 rate over a wide range of frequencies (MHz to mHz) at constant DC voltage equal to the open circuit voltage. These measurements were carried out for the electrochemical cells before and after cycling and results are summarized in Figure 9, with inset showing the equivalent circuit, used for fitting the experimental data using Zsimpwin program. The equivalent circuit consists of Re and Zw in series with two R-C circuits as the cathode-electrolyte and electrolyte-anode interface together with an addition capacitive Q element. The different resistances are extracted from these Nyquist plots and the data is summarized in Table 1.

The resistance values for the cells are considerably low in comparison with coin cells which were tested before cycling. This observation confirms that the conductivity has been improved after

cycling and helps for easier Li ions intercalation and de-intercalation which in turn improves the electrochemical performances like specific capacity and cyclic stability [1- 2]. This also explains the observed initial lower capacity in few cycles, as the resistance of cathode and interfaces were higher and thus, poor electronic/ionic transition resulted in relatively lower capacity in initial few cycles. The enhanced electronic/ionic conductivity observed for the combined with graphene cathode resulted in the increased discharge capacity and a high rate capability, facilitating the transfer of lithium ions across the active material/electrolyte interface, as well as the transfer of electrons from the current collector to the active material. In addition, the factors that may have contributed to the superior electrochemical performance of the graphene-containing cathode are improvement in the structural stability, a decrease in the disorder of metal ions in the lattice, and suppression of the dissolution of transition-metal ions and phase transitions. These results demonstrate that $LiMn_{1.5}Ni_{0.4}Cr_{0.1}O_4$ combined with graphene is suitable for application in advanced rechargeable lithium-ion batteries.

4. Conclusions:

Graphene modulated $LiMn_{1.5}Ni_{0.4}Cr_{0.1}O_4$ spinel structured composites were synthesized and tested for electrochemical performance. The structural stability of the $LiMn_{1.5}Ni_{0.4}Cr_{0.1}O_4$ was confirmed by XRD and ordered spinel structure with $p4_332$ symmetry confirmed by Raman spectroscopy. The FE-SEM images confirm homogenous orientation of graphene throughout the spinel structure. XPS investigation confirms that chromium and manganese ions changed their valence states from $Cr3^+$ to $Cr6^+$, whereas manganese changes from $Mn4^+$ to $Mn3^+$ state, during charging/discharging process. The discharge capacity of the graphene modulated $LiMn_{1.5}Ni_{0.4}Cr_{0.1}O_4$ at C/10 and C/2 discharge rates in the voltage range between 3.0 and 4.9 V obtained 150 mAh/g and 45 mAh/g respectively. In addition to the fast charge and discharge capability graphene modulated $LiMn_{1.5}Ni_{0.4}Cr_{0.1}O_4$ composite revealed promising cyclic stability, with 95% capacity retained after 50 cycles. In comparison with $LiMn_{1.5}Ni_{0.4}Cr_{0.1}O_4$, graphene modulated $LiMn_{1.5}Ni_{0.4}Cr_{0.1}O_4$ showed greatly improved electrochemical performance. The improved rate capability and cycling performance of graphene modulated $LiMn_{1.5}Ni_{0.4}Cr_{0.1}O_4$ cathode material attributed to an increase in the grain connectivity and high electronic conductivity for the smart hybrid electrode design.

Acknowledgements

This work was supported by the grant from NSF-CAWT project OIA-1849243

References

1. Armand M., Tarascon J.M. 2008 Building better batteries, Nature **451** 652–657.
2. Whittingham M.S., 2004 Lithium batteries and cathode materials, Chem. Rev. **104** 4271–4302.
3. Walter A., Schalkwijk Van**,** Scrosati Bruno, 2003 Advances in Li-ion batteris, J. Am. Chem. Soc. **125**(12) 3670-3671.
4. Tarascon J.M., Armand M, 2001 Issues and challenges facing rechargeable lithium batteries Nature **414** 359–367.
5. Ellis B.L., Lee K.T, Nazar L.F., 2010 Positive electrode materials for Li-ion and Li-batteries, Chem. Mater. **22** 691–714.
6. Goodenough J.B., Kim Y., 2010 Challenges for rechargeable Li batteries, Chem. Mater, **22** 587–603.
7. Xia Y, Zhou Y, Yoshio M., 1997 Capacity fading on cycling of 4 V Li/LiMn2 O 4 Cells, J. Electrochem. Soc. **144** 2593-2596.
8. Jang D.H., Shin J.Y., Oh S.M., 1996 Dissolution of spinel oxides and capacity losses in $LiMn_2O_4$ cells, J. Electrochem. Soc. **143** 2204-2210.
9. Gummow R.J., De Kock A., Thackeray M.M., 1994 Improved capacity retention in rechargeable 4 V lithium/lithium manganese oxide (spinel) cells, Solid State Ionics, **69** 59-67.
10. Cushing B.L., Goodenough J.B., 2002 Role of surface coating on cathode materials for lithium-ion batterie, Solid State Sci., **4** 1487–1493.
11. Wang D., Song C., Hu Z., and Fu Xun, 2005 Fabrication of hollow spheres and thin films of nickel hydroxide and nickel oxide with hirerchical structures, J. Phys. Chem. B, **109**(3) 1125-1129.
12. Singhal R, Aries J.J.S., Katiyar R., Ishikawa Y., Vilkas M.J., Das S.R., Tomar M.S., Katiyar R.S., 2009 High voltage spinel cathode materials for high energy density and high rate capability Li ion rechargeable batteries, J. Renew. Sustain. Energy **1** 023102.

13. Wei Y., Kim K.B., Chen G., 2006 Evolution of the local structure and electrochemical properties of spinel $LiNi_xMn_{2-x}O_4$ ($0 \leq x \leq 0.5$), Electrochem. Acta. **51** 3365-3370.

14. Yoon Y.K., Park C.W., Ahn H.Y., Kim D.H., Lee Y.S., Kim J., 2007 Synthesis and characterization of spinel type high poer cathode materials $LiM_xMn_{2-x}O_4$ J. Phys. Chem. Solids **68** 780-784.

15. Suryakala K, Kalaignan G.P., Vasudevan T., 2007 Structural and Electrochemical Study of New $LiNi_{0.5}Ti_xMn_{1.5-x}O_4$ Spinel Oxides for 5-V Cathode Materials, Mater. Chem. Phys. **104** 479-483.

16. Thackeray M.M., David W.I.F., Bruce P.G., Goodenough J.B., 1983 Lithium insertion into manganese spinels , Mater. Res. Bull. **18** 461-472.

17. Wu E., 2005 POWDMULT, version 2.1, An Interactive Powder Diffraction Data Interpretation and Indexing Program, School of Physical Science, Flinders University of South Australia, Bedford Park, South Australia 5042 .

18. Bao S.J., Liang Y.Y., Li H.L., 2005 Synthesis and electrochemical properties of LiMn2O4 by microwave-assisted sol–gel method, Mater. Lett. **59** 3761-3765.

19. Park S.B., Eom W.S., Cho W.I., Jang H., 2006 Electrochemical properties of $LiNi_{0.5}Mn_{1.5}O_4$ cathode after Cr doping, J. Power Sources **159** 679-684.

20. Wu Q.H., Xu J.M., Zhuang Q.C., Sun S.G., 2006 X-ray photoelectron spectroscopy of LiM0.05Mn1.95O4 (M=Ni, Fe and Ti), Solid State Ionics **177** 1483-1486.

21. Shaju K.M., Subba Rao G.V., Chowdari B.V.R., 2002 Influence of Li-Ion Kinetics in the Cathodic Performance of Layered $Li(Ni_{1/3}Co_{1/3}Mn_{1/3})O_2$, Solid State Ionics, **60** 152–153.

22. Soroosh S. A., Fernando A., Soto T.F., Mohammad A., Yuan Y., Ramasubramonian D., Rojaee R., Song B., Khalil X.B., Lu A.J., Khojin A.S., Balbuena P.B., Yassar R.S. 2019 Anti-Oxygen Leaking $LiCoO_2$. Advanced Functional Materials, **1901110**,1-12**.**

23. Tian P., Tang L., Teng K.S., Lau S.P., 2018 Graphene quantum dots from chemistry to applications, Materials Today Chemistry,**10**, 221-**258.**

24. Liang G., Peterson V.K., See K.W., Guo Z., Pang W.K. 2020 Developing high-voltage spinel $LiNi_{0.5}Mn_{1.5}O_4$ cathodes for high-energy-density lithium-ion batteries: current achievements and future prospects, Journal of materials Chemistry A, **1039**, 1-53.

25. Dong H., Zhang Y., Zhang S., Tang P., Xiao X., Ma M., Zhang H., Yin Y., Wang D., Yang S. 2019 Improved High Temperature Performance of a Spinel $LiNi_{0.5}Mn_{1.5}O_4$ Cathode for High-Voltage Lithium-Ion Batteries by Surface Modification of a Flexible Conductive Nanolayer, *ACS Omega*, **4** 185-194.
26. Tang X., Jan S.S., Qian Y., Xia H., Ni J., Savilov S.V., Aldoshin S.M. 2015Graphene wrapped ordered $LiNi_{0.5}Mn_{1.5}O_4$ nanorods as promising cathode material for lithium-ion batteries, Sci Rep. **5**: 11958-11967.
27. Aklaloucha M., Amarillaa J.M., Rojas R.M., Saadoune I., Rojo J.M., 2008 High voltage spinel cathode materials for high energy density and high rate capability Li ion rechargeable batteries, J. Power Sources **185** 501-508.
28. Xu X.X., Yang J., Wang Y.Q., NuLi Y.N., Wang J.L., 2007 LiNi0.5Mn1.5O3.975F0.05 as novel 5 V cathode material, J. Power Sources **174** 1113-1117.
29. Jeong I.S., Kim J.U., Gu H.B., 2001 Synthesis of Al-doped $LiMn_2O_4$ spinels by mechanical alloying and rotary heating, J. Power Sources **102** 55-60.
30. Katiyar R.K. , Singhal R. , Asmar K. , Valentin R. , Katiyar Ram S, 2009 High voltage spinel cathode materials for high energy density and high rate capability Li ion rechargeable batteries, Journal of Power Sources **194** 526–530.
31. Hwang B.J.,Tsai Y.W.,Carlier D., Ceder G., 2003 A Combined computational/Experimental Study on LiNi1/3Co1/3Mn1/3O_2, Chem. Mater., **15** 3676–3682.
32. Reddy A.L.M., Srivastava A, Gowda S.R., Gullapalli H., Dubey M., Ajayan P.M., 2010 Synthesis Of Nitrogen-Doped Graphene Films For Lithium Battery Application, ACS Nano **4** 6337–6342.
33. Venkateswara Rao Ch., Reddy A.L.M., Ishikawa Y., Ajayan P.M., 2010 $LiNi_{1/3}Co_{1/3}Mn_{1/3}O_2$–Graphene Composite as a Promising Cathode for Lithium-Ion Batteries, Carbon, **49** 931–936.
34. Gao W., Alemany L., 2009 Ajayan P.M., New insights into the structure and reduction of Graphite Oxide, Nat. Chem. **1** 403–408.
35. Wang L., Li H, Huang X, & Baudrin E., 2011 A comparative study of Fd-3m and p4,32 LiNi0.5Mn1.5O4, Solid State Ionics, **193** 32-38.

36. Liu J. and Manthiram A., 2009 Understanding the improvement in the electrochemical Properties of Surface Modified 5 V $LiMn_{1.42}Ni_{0.42}Co_{0.16}O_4$ Spinel Cathodes in Lithium-ion Cells, Chem. Mater., **21** 1695-1699.
37. Funabiki A, Inaba M, and Ogumi Z, 1997 AC impedance analysis of electrochemical lithium intercalation into highly oriented pyrolytic graphite, J. Power Source, **68** 227-232.
38. Oswald S, Nikolowski K. and Ehrenberg H.**,** 2010 XPS investigations of valence changes during cycling of $LiCrMnO_4$-based cathodes in Li-ion batteries, Surf. Interface Anal. **42** 916–921.
39. Li B., Cao H, Shao J., Zheng H., Lu Y., Yin J., Qu M., 2011 Improved performance of beta-Ni(OH)2 reduced grapheme oxide in Ni-MH and Li-ion batteries, Chem. Commun. **47** 3159-3161.
40. Jia X, Yan C, Chen Z., Wang R., Zhang Q., Guo L., Wei F., Lu Y., 2011 Direct growth of flexible LiMn2O4/CNT lithium ion cathodes, Chem. Commun. **47** 9669-9671.36.
41. Ven Vander A., Marianetti C., Morgan D., Ceder G., 2000 Phase transformations and volume changes in spinel $Li_2Mn_2O_4$, Solid State Ionics, **135** 21-32.
42. Zhang J., Yang H., Shen G., Cheng P., Zhang J., Guo S., 2010 Reduction of grapheme oxide via L-ascorbic acid, Chem. Commun. **46** 1112-1114.
43. Shi T., Dong Y., Wang C.M., Tao F., Chen L., 2015 Enhanced cyclic stability at high rate and excellent high rate capability of $La_{0.7}Sr_{0.3}Mn_{0.7}Co_{0.3}O_3$ coated LiMn2O4, J. Power Sources **273** 959-965.

Figure captions

Fig.1. X-ray diffraction spectrum of grapheme modulated $LiMn_{1.5}Ni_{0.4}Cr_{0.1}O_4$ cathode

Fig.2.Raman spectra at 514 nm for $LiMn_{1.5}Ni_{0.4}Cr_{0.1}O_4$ and $LiMn_{1.5}Ni_{0.4}Cr_{0.1}O_4$ graphene: (a) pristine $LiMn_{1.5}Ni_{0.4}Cr_{0.1}O_4$(b) a $LiMn_{1.5}Ni_{0.4}Cr_{0.1}O_4$ graphene in the range 200-2500 cm^{-1} and (c) spectra in the region of $LiMn_{1.5}Ni_{0.4}Cr_{0.1}O_4$, graphene D and G bands.

Fig.3. Surface morphologies of (a) pure $LiMn_{1.5}Ni_{0.4}Cr_{0.1}O_4$ (b-d) graphene modulated $LiMn_{1.5}Ni_{0.4}Cr_{0.1}O_4$ cathode material studied by FE-SEM.

Fig.4. Cyclic voltammogram of graphene modulated $LiMn_{1.5}Ni_{0.4}Cr_{0.1}O_4$ cathode material /LiPF6 + (EC + DMC)/Li coin cell in 3.0–4.9 V range, at a voltage scan rate of 0.1 mV s^{-1}.

Fig.5. XPS spectra of graphene modulated $LiMn_{1.5}Ni_{0.4}Cr_{0.1}O_4$ cathode material before cycling black legend and after cycling in red legend.

Fig.6. Charge/discharge cycles of graphene modulated $LiMn_{1.5}Ni_{0.4}Cr_{0.1}O_4$ cathode material /LiPF6 + (EC + DMC)/Li coin cell in 3.0–4.9 V range, at C/10- rate.

Fig.7. Charge/discharge cycles of graphene modulated $LiMn_{1.5}Ni_{0.4}Cr_{0.1}O_4$ cathode material /LiPF6 + (EC + DMC)/Li coin cell in 3.0–4.9 V range, at C/2- rate.

Fig.8. Stability of graphene modulated $LiMn_{1.5}Ni_{0.4}Cr_{0.1}O_4$ cathode material /LiPF6 + (EC + DMC)/Li coin cell at C/10 and C/2 in range of (1-50 cycles).

Fig.9.Impedance spectra of graphene modulated $LiMn_{1.5}Ni_{0.4}Cr_{0.1}O_4$ cathode material /$LiPF_6$ + (EC + DMC)/Li coin cell: (a) before charge/discharge and (b) after 50 charge/discharge cycles.

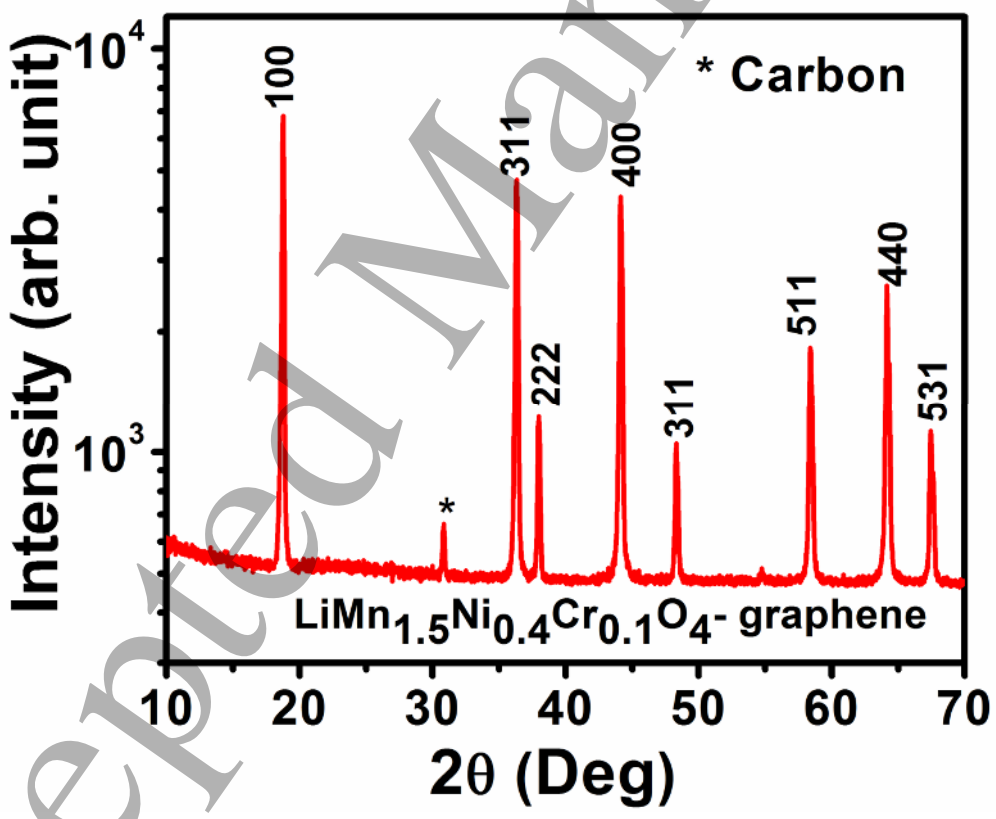

Figure 1. X-ray diffraction spectrum of graphene modulated $LiMn_{1.5}Ni_{0.4}Cr_{0.1}O_4$ cathode

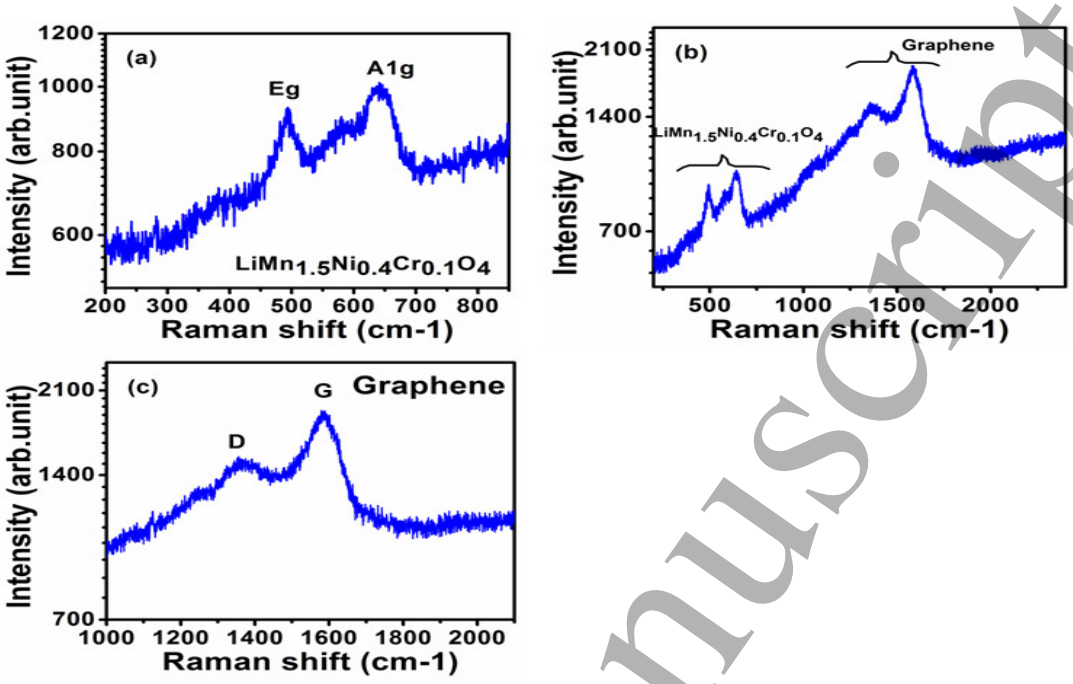

Fig.2.Raman spectra at 514 nm for $LiMn_{1.5}Ni_{0.4}Cr_{0.1}O_4$ and $LiMn_{1.5}Ni_{0.4}Cr_{0.1}O_4$ graphene: (a) pristine $LiMn_{1.5}Ni_{0.4}Cr_{0.1}O_4$(b) a $LiMn_{1.5}Ni_{0.4}Cr_{0.1}O_4$ graphene in the range 200-2500 cm^{-1} and (c) spectra in the region of $LiMn_{1.5}Ni_{0.4}Cr_{0.1}O_4$, graphene D and G bands

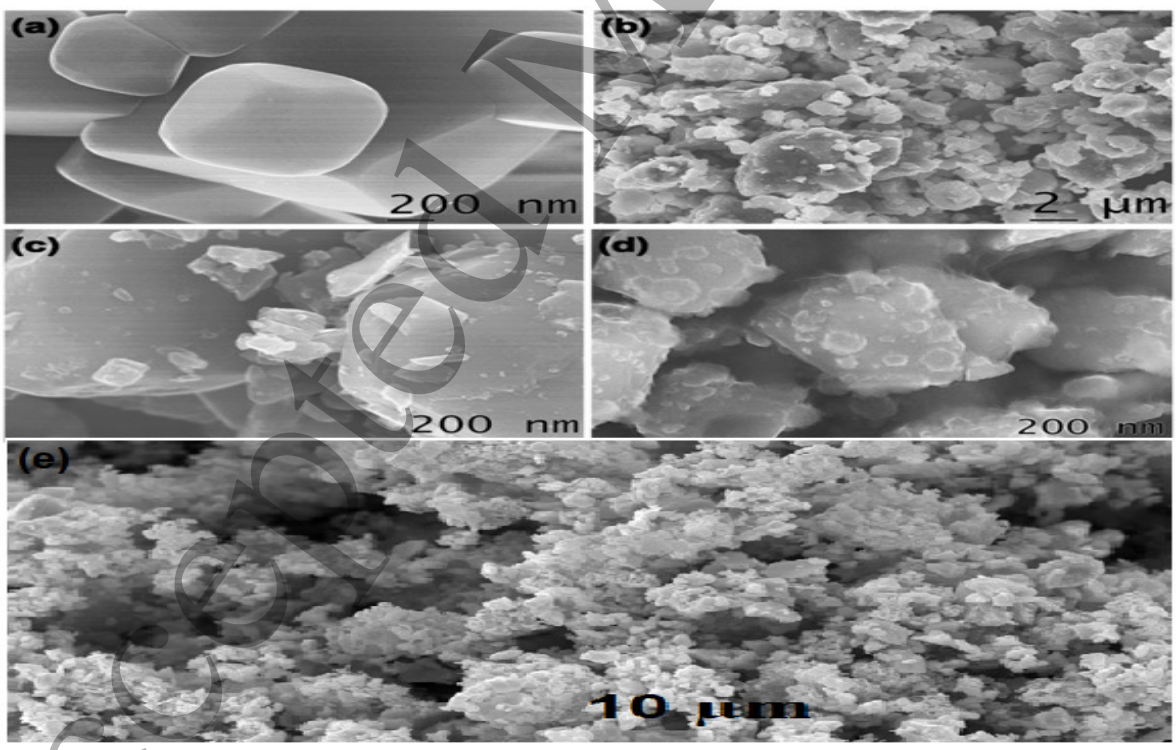

Fig.3. Surface morphologies of (a) pure $LiMn_{1.5}Ni_{0.4}Cr_{0.1}O_4$ (b-c-d-e) graphene modulated $LiMn_{1.5}Ni_{0.4}Cr_{0.1}O_4$ cathode material studied by FE-SEM

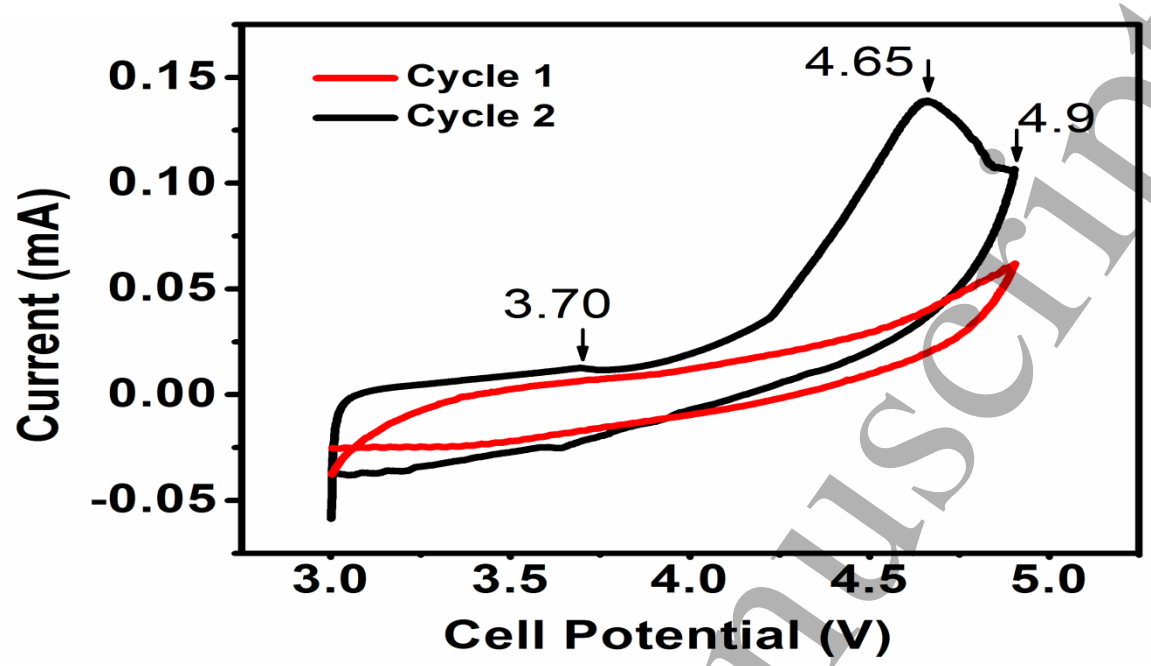

Fig.4. Cyclic voltammogram of $LiMn_{1.5}Ni_{0.4}Cr_{0.1}O_4$ combined with graphene cathode material /LiPF6 + (EC + DMC)/Li coin cell in 3.0–4.9 V range, at a voltage scan rate of 0.1 mV s^{-1}.

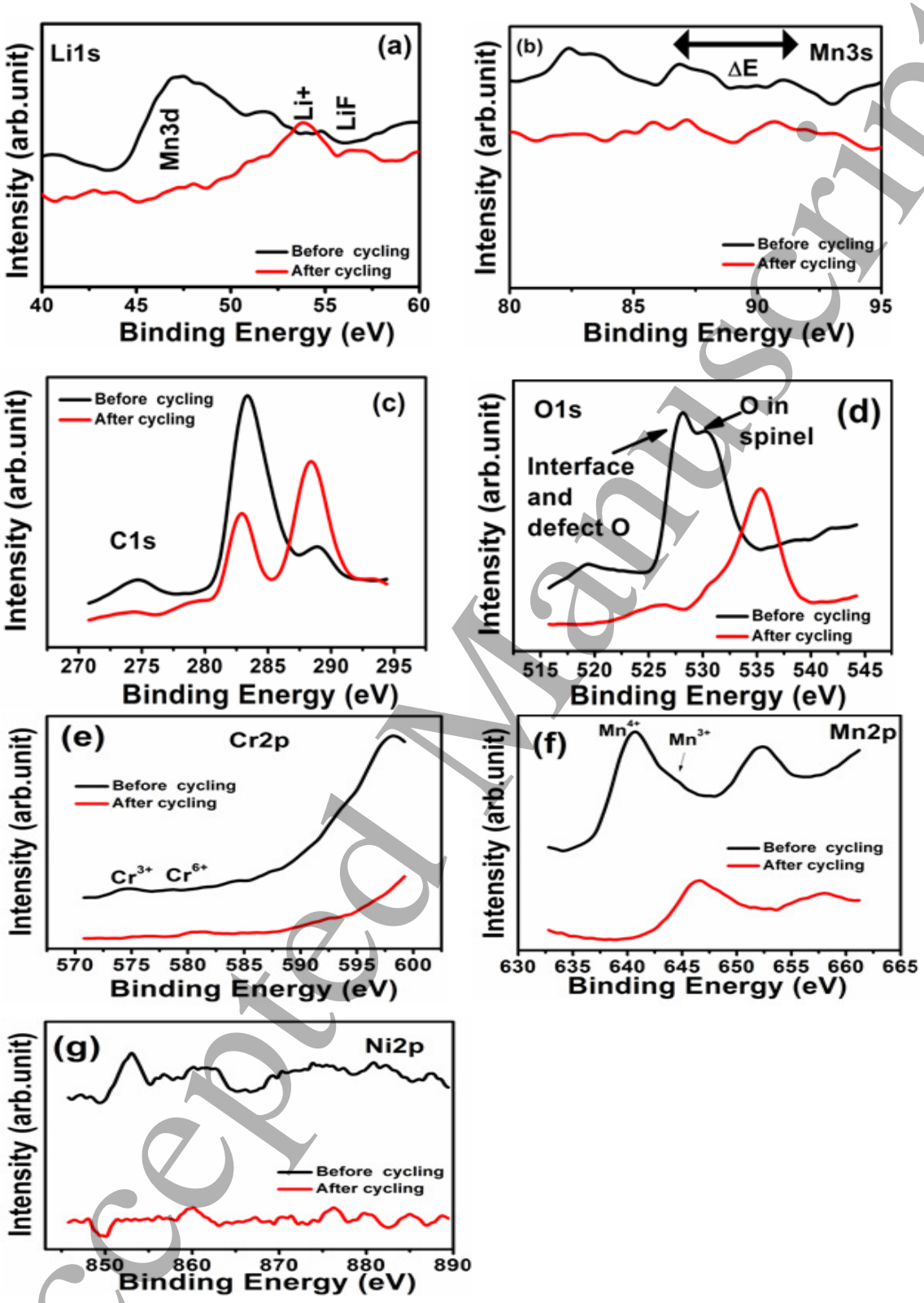

Fig.5. XPS spectra of graphene modulated $LiMn_{1.5}Ni_{0.4}Cr_{0.1}O_4$ cathode material before cycling black legend and after cycling in red legend

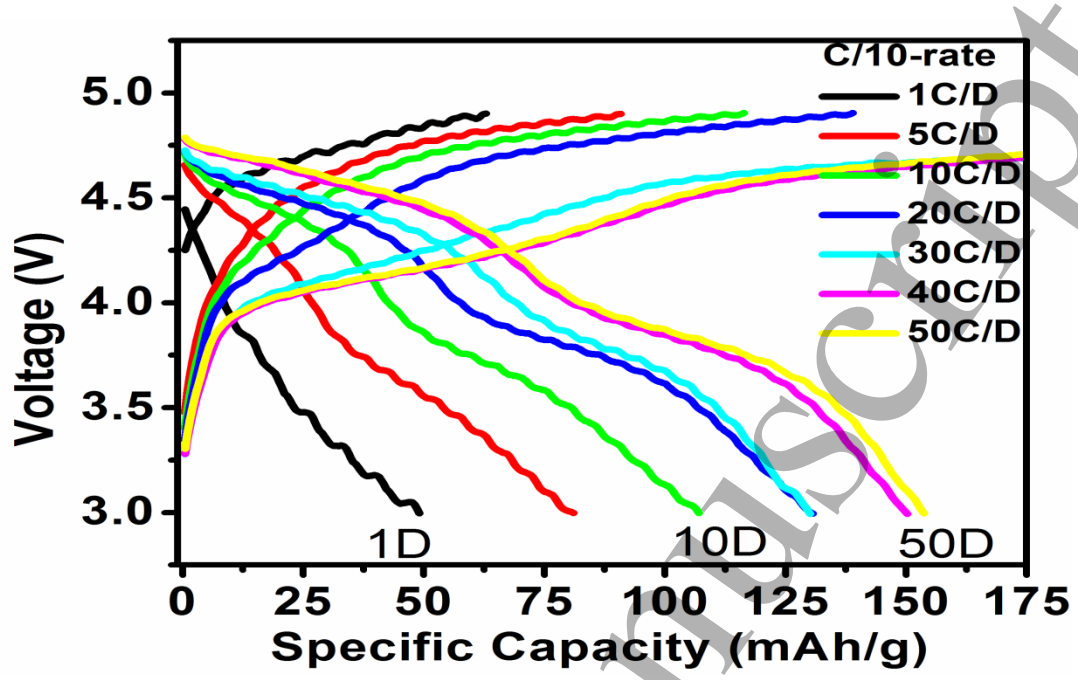

Fig.6. Charge/discharge cycles of $LiMn_{1.5}Ni_{0.4}Cr_{0.1}O_4$ combined with graphene cathode material /LiPF6 + (EC + DMC)/Li coin cell in 3.0–4.9 V range, at C/10- rate.

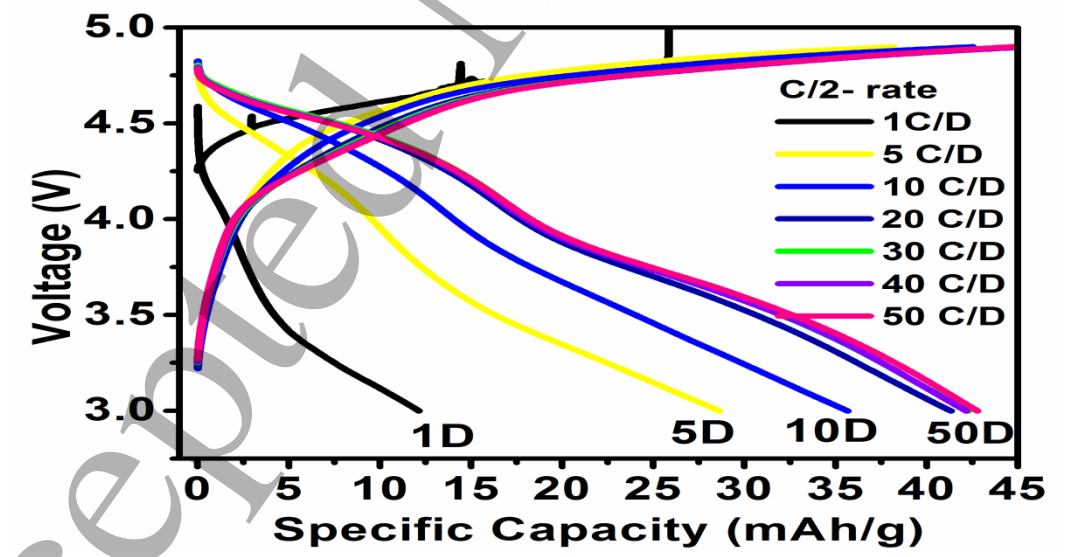

Fig.7. Charge/discharge cycles of graphene modulated $LiMn_{1.5}Ni_{0.4}Cr_{0.1}O_4$ cathode material /LiPF6 + (EC + DMC)/Li coin cell in 3.0–4.9 V range, at C/2- rate

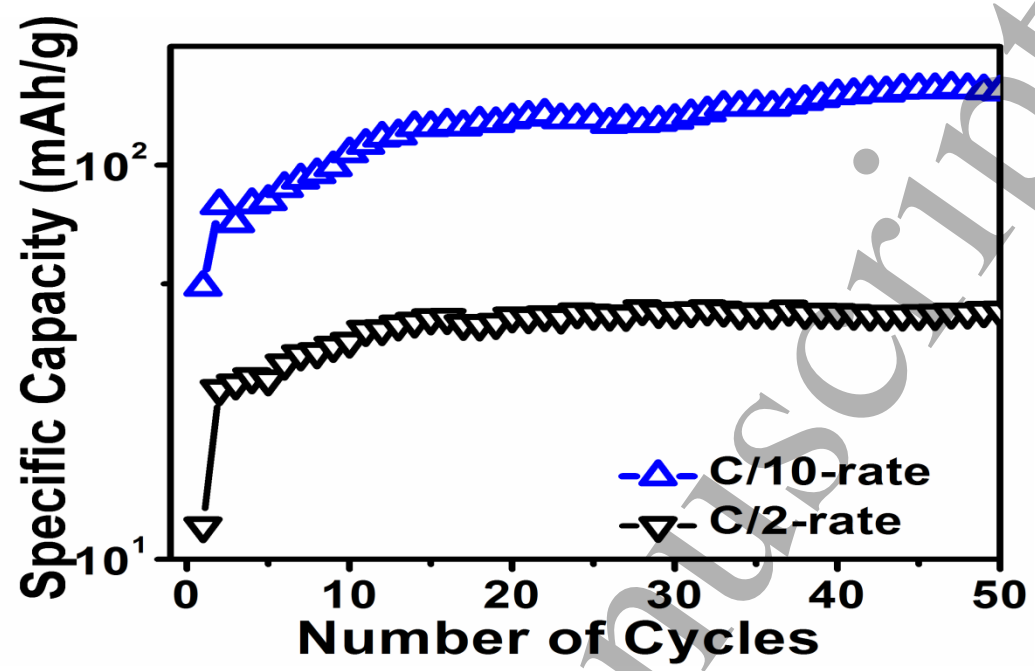

Fig.8. Stability of graphene modulated $LiMn_{1.5}Ni_{0.4}Cr_{0.1}O_4$ cathode material /LiPF6 + (EC + DMC)/Li coin cell at C/10 and C/2 in range of (1-50 cycles).

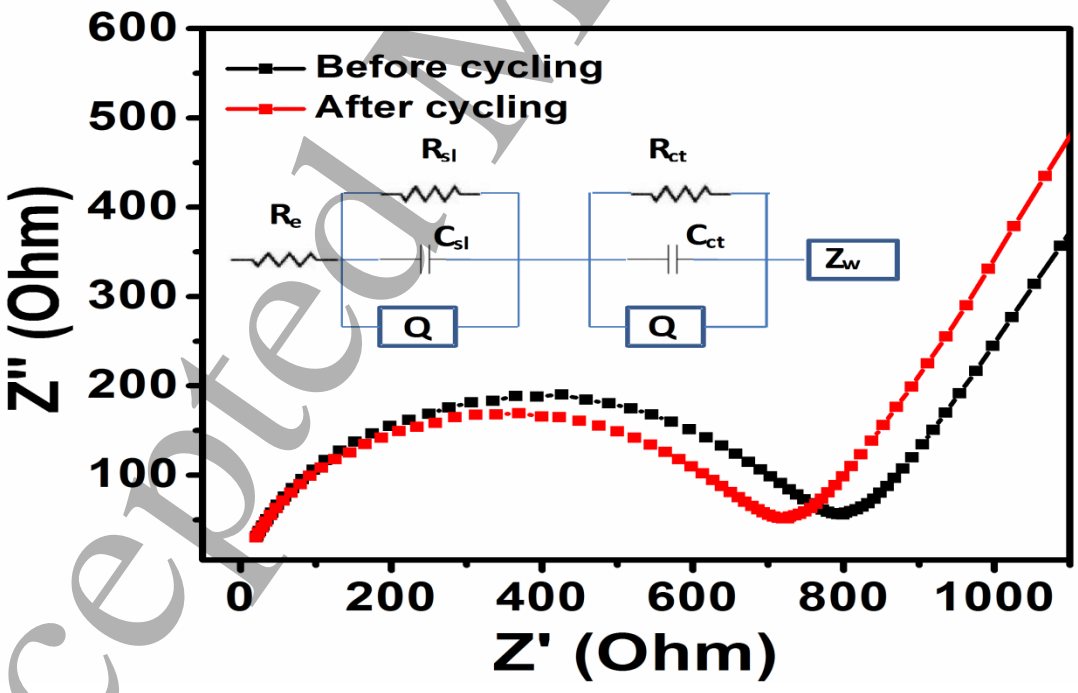

Fig.9.Impedance spectra of grapheme modulated $LiMn_{1.5}Ni_{0.4}Cr_{0.1}O_4$ cathode material /$LiPF_6$ + (EC + DMC)/Li coin cell: (a) before charge/discharge and (b) after 50 charge/discharge cycles